

## Enhancement of photocatalytic activity from $\text{HCa}_2\text{Ta}_x\text{Nb}_{3-x}\text{O}_{10}$ ( $x=0, 1$ ), co-intercalated with sulfides particles



Yuelin Wei<sup>a</sup>, Xiaopei Zhang<sup>a,b</sup>, Jing Xu<sup>a,b</sup>, Jing Wang<sup>a,b</sup>, Yunfang Huang<sup>a,b,\*</sup>,  
Leqing Fan<sup>a</sup>, Jihuai Wu<sup>a</sup>

<sup>a</sup> Engineering Research Center of Environment-Friendly Functional Materials, Ministry of Education, Huaqiao University, Xiamen 361021, China

<sup>b</sup> College of Chemical Engineering, Huaqiao University, Xiamen 361021, China

### ARTICLE INFO

#### Article history:

Received 18 August 2013

Received in revised form 4 October 2013

Accepted 12 October 2013

Available online 18 October 2013

#### Keywords:

Photocatalysis

Hydrogen production

Layered perovskite  $\text{HCa}_2\text{Ta}_x\text{Nb}_{3-x}\text{O}_{10}$  ( $x=0, 1$ )

Co-intercalation

### ABSTRACT

A novel heterogeneous photocatalysts  $\text{HCa}_2\text{Ta}_x\text{Nb}_{3-x}\text{O}_{10}/(\text{ZnS, PbS})$  ( $x=0, 1$ ) were fabricated by intercalation and exchange reactions. The physicochemical properties of the photocatalysts were analyzed by Scanning Electron Microscopy (SEM), X-ray Diffraction (XRD), Ultraviolet-visible spectroscopy (UV-Vis), Fourier transformed infrared spectra (FT-IR) and Photoluminescence technique (PL). The photocatalytic activity of the  $\text{HCa}_2\text{Ta}_x\text{Nb}_{3-x}\text{O}_{10}/(\text{ZnS, PbS})$  was evaluated by photocatalytic  $\text{H}_2$  production in an aqueous solution containing  $\text{SO}_3^{2-}$  and  $\text{S}^{2-}$  as a sacrificial agent under UV light irradiation.  $\text{HCa}_2\text{Ta}_x\text{Nb}_{3-x}\text{O}_{10}/(\text{ZnS, PbS})$  possessed a higher gallery height than that of  $\text{HCa}_2\text{Ta}_x\text{Nb}_{3-x}\text{O}_{10}$ , which indicated the formation of an intercalated nanomaterial and a heterogeneous catalyst. The results showed that these samples presented strong photocatalytic activity even without co-catalyst noble metal Pt. The photocatalytic activity of  $\text{HCa}_2\text{Ta}_x\text{Nb}_{3-x}\text{O}_{10}/(\text{ZnS, PbS})$  was several times higher than that of unsupported  $\text{HCa}_2\text{Ta}_x\text{Nb}_{3-x}\text{O}_{10}$ . The heterogeneous electron transfer from guest ZnS, PbS to host  $\text{HCa}_2\text{Ta}_x\text{Nb}_{3-x}\text{O}_{10}$  layer and the substitution of Ta for partial Nb seemed to play an important role to enhance the photocatalytic activity.

© 2013 Elsevier B.V. All rights reserved.

### 1. Introduction

The photocatalytic production of hydrogen from water using semiconductor materials is of great interest from both theoretical and practical point of view due to its possible application for converting the sunlight energy into chemical energy [1,2]. In the past decades, among the various photocatalytic materials available, metal oxides, such as  $\text{TiO}_2$  and  $\text{ZnO}$ , have been widely investigated and used because they are inexpensive, chemically stable, nontoxic, and possess favorable optoelectronic properties [3,4]. Unfortunately, the photo-efficiency of a single band-gap material is too low by its relatively wide band-gap restricting its absorption of solar energy. It is a great challenge to synthesize the catalyst which is active under sun light irradiation. Many studies have been carried out by modification of photocatalyst materials with dye sensitization, doping ions, the control of the band structure, and chemical substitution for semiconducting metal oxides [5–7].

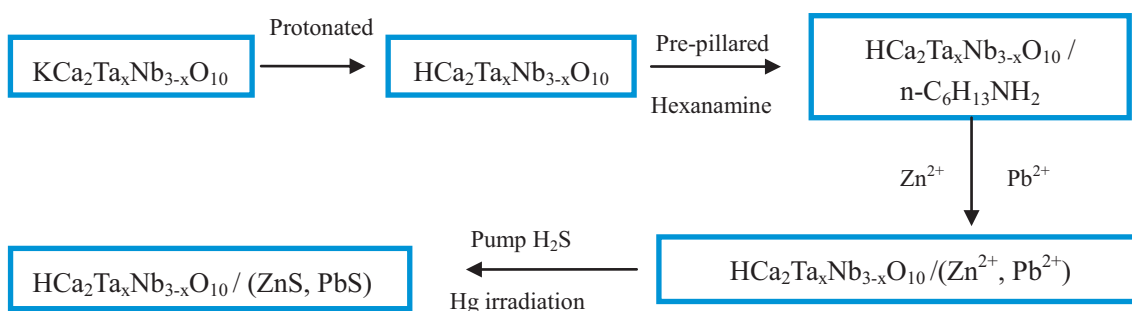
Recently, titanium- and niobium-based lamellar perovskite photocatalyst has attracted attention as a novel strategy for improving the efficiency of photocatalysts [8–12]. There are two different typical structures, the Dion–Jacobson

series ( $\text{A}'[\text{A}_{n-1}\text{B}_n\text{O}_{3n+1}]$ ) and the Ruddlesden–Popper series ( $\text{A}'_2[\text{A}_{n-2}\text{B}_n\text{O}_{3n+1}]$ ). Their orthorhombic layered structure is composed of corrugated host layers of edge-shared octahedra and interlayer alkali metal ions compensating for the minus charge which arises from substitution of lower valence metal ions or vacancies for Ti or Nb. These alkali metal ions are exchangeable with a variety of inorganic and organic cations, providing an opportunity to modify chemical and physical properties. Compared with the common bulk metal oxide photocatalysts, lamellar perovskite photocatalysts are more promising: The valence band top and the conduction band bottom are located at desirable potential levels, the layered structure facilitates electron transfer, and the protonic acidity is favorable for water and some organic molecules adsorption. One interesting feature of these complex mixed-oxides is that their catalytic activities can be highly improved by partial substitution on A- and/or B-sites, with only small changes in the crystal structure.

Metal sulfides are well-known semiconductor photocatalysts for hydrogen evolution from aqueous solutions containing sacrificial reagents of  $\text{Na}_2\text{S}$  and  $\text{Na}_2\text{SO}_3$ , and several breakthroughs in their use have been achieved [13–15]. PbS is an indirect band gap semiconductor with a bulk band gap of about 0.41 eV [16]. So it can absorb the light in the whole visible region, and thus, is very attractive from the viewpoint of efficient solar energy utilization. It has smaller effective masses of charge carriers, high value of dielectric

\* Corresponding author. Tel.: +86 592 6162300; fax: +86 592 6162300.

E-mail address: [huangyf@hqu.edu.cn](mailto:huangyf@hqu.edu.cn) (Y. Huang).

**Scheme 1.** Schematic procedure of preparing the catalysts.

constant, and a fairly high value of excitonic Bohr radius ( $\sim 20$  nm). For these reasons it allows strong quantum confinement even in relatively large PbS quantum dots [17]. More interestingly, the recent discovery of the multiple exciton generation effect in some lead salts including PbS QDs opens up the possibility of overcoming the ordinary thermodynamic limits of solar energy conversion [18].

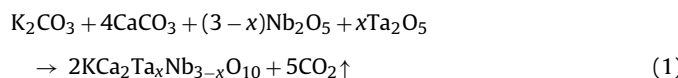
ZnS is another important semiconductor material investigated for photocatalytic water splitting compared to those of TiO<sub>2</sub> [19,20]. ZnS nano-crystals are good photocatalysts as a result of the rapid generation of electron hole pairs by photo-excitation and highly negative reduction potentials of excited electrons. The ternary/coupled semiconductor systems such as Pt-PdS/CdS [14], ZnS/CdS/ZTP [21], (CdS-ZnS)TiO<sub>2</sub> [22], are known to exhibit higher photocatalytic activity as compared to their constituent sulfides or oxides. A number of interesting electronic features have been observed in these studies. It is still a challenging task to synthesize and understand such nanocomposites thoroughly in terms of interaction between its different components and to examine dynamics of charge carriers under irradiation for their better utilization as photocatalytic materials. So we expect to enhance stability and light-harvesting properties by co-incorporating the nanoparticles of PbS and ZnS into the interlayer of lamellar perovskite photocatalysts.

It is well-known that loading of Pt on TiO<sub>2</sub> has high hydrogen production efficiency for photocatalytic water splitting in the presence of sacrificial reagents [23]. However, Pt is a rare and expensive noble metal. Herein, we report the preparation of ZnS and PbS nanoparticles co-intercalated HCa<sub>2</sub>Ta<sub>x</sub>Nb<sub>3-x</sub>O<sub>10</sub> ( $x = 0, 1$ ) without co-catalyst noble metal Pt for photocatalytic H<sub>2</sub> production using Na<sub>2</sub>S and Na<sub>2</sub>SO<sub>3</sub> as sacrificial agents.

## 2. Experimental

### 2.1. Preparation of samples

The preparation procedure of the catalyst was shown in **Scheme 1**. The layered compound KCa<sub>2</sub>Ta<sub>x</sub>Nb<sub>3-x</sub>O<sub>10</sub> was prepared by conventional solid-state reactions [24]. All regents used were from Sinopharm Chemical Reagent Co., Ltd with no further purification. The starting materials of K<sub>2</sub>CO<sub>3</sub>, Ta<sub>2</sub>O<sub>5</sub>, Nb<sub>2</sub>O<sub>5</sub> and CaCO<sub>3</sub> powders were ground in a stoichiometric ratio according to the following equation. The excess amount of potassium carbonate (20 mol%) was added in the mixture to compensate its volatilization.



The mixture was calcined at 1150 °C for 24 h in air one intermediate regrinding in 12 h. The product was washed with distilled water to remove the excess of the alkaline component, and then

dried at 105 °C to obtain KCa<sub>2</sub>Ta<sub>x</sub>Nb<sub>3-x</sub>O<sub>10</sub> anhydrous compound. HCa<sub>2</sub>Ta<sub>x</sub>Nb<sub>3-x</sub>O<sub>10</sub> was carried out by proton exchange reaction of KCa<sub>2</sub>Ta<sub>x</sub>Nb<sub>3-x</sub>O<sub>10</sub> in HCl (1 mol L<sup>-1</sup>) solution at 60 °C for 96 h, with intermediate replacement of the acid in 24 h. After the reaction, the deposit product was washed to remove the excess of the acid component and then air-dried. The washed water was tested for K<sup>+</sup> content by atomic absorption spectrophotometer (PERKIN-ELMER1100B). The ion exchange ratio for hydrogen to potassium was ca. 95% for 24 h and nearly 100% for 96 h.

In order to incorporating ZnS and PbS nanoparticles into the interlayer of HCa<sub>2</sub>Ta<sub>x</sub>Nb<sub>3-x</sub>O<sub>10</sub>, the interlayer of HCa<sub>2</sub>Ta<sub>x</sub>Nb<sub>3-x</sub>O<sub>10</sub> was pre-expanded by the intercalation of *n*-C<sub>6</sub>H<sub>13</sub>NH<sub>2</sub> long chain molecule. The alkylammonium intercalation reaction was carried out at room temperature by an acid-base reaction. HCa<sub>2</sub>Ta<sub>x</sub>Nb<sub>3-x</sub>O<sub>10</sub>/n-C<sub>6</sub>H<sub>13</sub>NH<sub>2</sub> was obtained by stirring HCa<sub>2</sub>Ta<sub>x</sub>Nb<sub>3-x</sub>O<sub>10</sub> in *n*-C<sub>6</sub>H<sub>13</sub>NH<sub>2</sub>/C<sub>2</sub>H<sub>5</sub>OH (20 vol%) mixture solution under reflux at 60 °C for 72 h after filtered, washed and dried. Then, the HCa<sub>2</sub>Ta<sub>x</sub>Nb<sub>3-x</sub>O<sub>10</sub>/n-C<sub>6</sub>H<sub>13</sub>NH<sub>2</sub> individually dispersed into the Zn(CH<sub>3</sub>COO)<sub>2</sub> and Pb(CH<sub>3</sub>COO)<sub>2</sub> mixed solutions with equimolar ratios (0.1 mol L<sup>-1</sup>) to form a mixed suspension, and stirred at 70 °C for 72 h. In order to remove excess Zn<sup>2+</sup> and Pb<sup>2+</sup> on the outer surface, the sediment was filtered and washed with distilled water until no Zn<sup>2+</sup> or Pb<sup>2+</sup> was detected in elute solution then dispersed in deionized water to form a new suspension. The residual Zn<sup>2+</sup> or Pb<sup>2+</sup> concentration was detected by 0.1 mol dm<sup>-3</sup> Na<sub>2</sub>S solution. The new suspension was placed in a sealed round-bottom flask, and excess H<sub>2</sub>S gas was slowly bubbled into the flask under vigorous stirring for 3 h. The excess H<sub>2</sub>S gas was dissolved in amine solvents. After being filtered and washed with water, the specimen was dispersed in water and irradiated with UV light from a 100 W high-pressure mercury lamp at room temperature at 60 °C for 8 h so as to decompose any *n*-C<sub>6</sub>H<sub>13</sub>NH<sub>2</sub> remaining in the interlayer of HCa<sub>2</sub>Ta<sub>x</sub>Nb<sub>3-x</sub>O<sub>10</sub>. The sample obtained was designated as HCa<sub>2</sub>Ta<sub>x</sub>Nb<sub>3-x</sub>O<sub>10</sub> / (ZnS, PbS), HCa<sub>2</sub>Ta<sub>x</sub>Nb<sub>3-x</sub>O<sub>10</sub> / (Zn<sup>2+</sup>, Pb<sup>2+</sup>)

### 2.2. Characterization

Purity and crystallinity phases of the products were identified by powder X-ray diffraction on Bruker D8-advance X-ray diffractometer (XRD) at 40 kV and 30 mA for monochromatized Cu-K<sub>α</sub> ( $\lambda = 0.154$  nm) radiation. The micromorphology of samples was observed by field-emission scanning electron microscope (FE-SEM, Hitachi S-4800N). The composition of samples was measured by the energy dispersive X-ray spectrometer (EDS, INCA, Oxford Co., U.K.). The band gap energies of the products were determined from the onset of diffuse reflectance spectra of the powders measured using a Shimadzu Model UV-3100 UV-vis spectrophotometer. The Fourier infrared spectra (FT-IR) of the samples were measured with a Nicolet-470 Fourier transform infrared spectrometer by the KBr method. Fluorescence of samples was measured by Varian Cary Eclipse Fluorescence Spectrophotometer, and the scanning rate

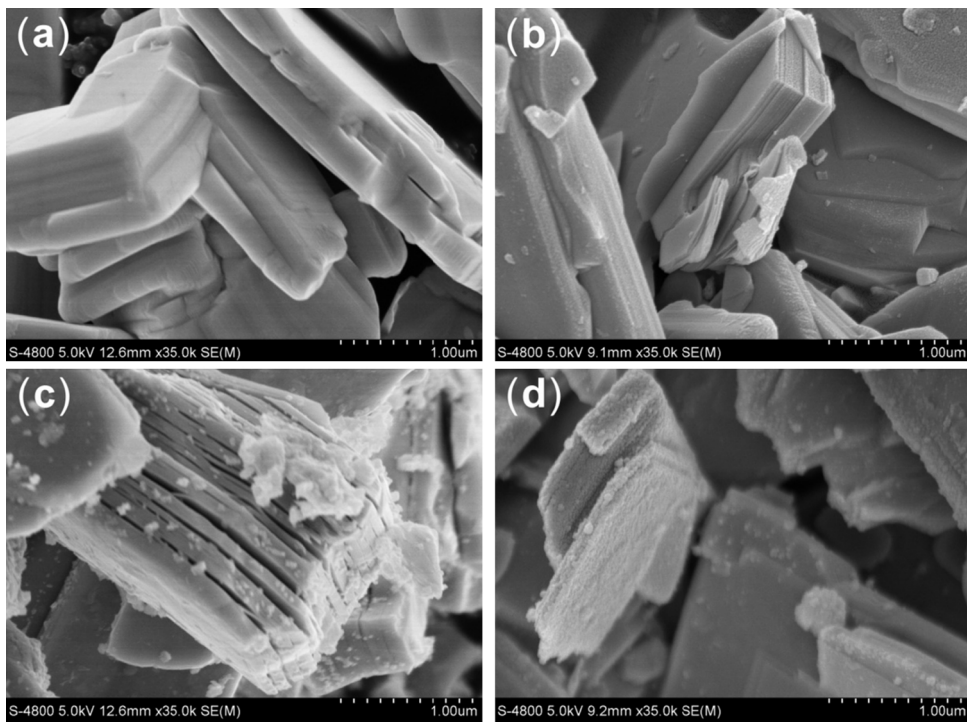


**Fig. 1.** SEM images of (a) HCa<sub>2</sub>Nb<sub>3</sub>O<sub>10</sub>, (b) HCa<sub>2</sub>TaNb<sub>2</sub>O<sub>10</sub>, (c) HCa<sub>2</sub>Nb<sub>3</sub>O<sub>10</sub>/(ZnS, PbS), and (d) HCa<sub>2</sub>TaNb<sub>2</sub>O<sub>10</sub>/(ZnS, PbS).

was 600 nm/min. The element contents were determined by atomic emission spectroscopy (Intertid xsp radil ict-aes).

### 2.3. Photocatalytic activity measurement

Photocatalytic reaction was carried out in a Pyrex reactor of 500 cm<sup>3</sup> capacity attached to an inner radiation type a 300 W high-pressure mercury lamp. The inner cell had thermostat water flowing through a jacket between the mercury lamp and the reaction chamber. The inner cell was constructed with Pyrex glass, which served to filter out the UV emission of a 300 W mercury lamp with wavelengths less than 290 nm. The photocatalytic activities of sample were determined by measuring the volume of hydrogen gas evolved from 500 cm<sup>3</sup> of the mixed aqueous solution of Na<sub>2</sub>S (0.2 mol dm<sup>-3</sup>) and Na<sub>2</sub>SO<sub>3</sub> (0.2 mol dm<sup>-3</sup>) aqueous solution as the sacrificial reagents containing 1.0 g of dispersed samples at 60 °C with a gas burette, respectively. Prior to the reaction, the mixture was deaerated by evacuation and then flushed with N<sub>2</sub> (20 kPa) repeatedly to remove O<sub>2</sub> and CO<sub>2</sub> dissolving in water. Before irradiation, it was confirmed that no reaction occurred in the dark. The evolved gas was analyzed by gas chromatography (Shanghai, 102G, molecular sieve 5A column and Ar carrier).

## 3. Results and discussion

### 3.1. Scanning electron microscopy

The particle size and the morphologies of the as-prepared HCa<sub>2</sub>Nb<sub>3</sub>O<sub>10</sub>, HCa<sub>2</sub>TaNb<sub>2</sub>O<sub>10</sub>, HCa<sub>2</sub>Nb<sub>3</sub>O<sub>10</sub>/(ZnS, PbS) and HCa<sub>2</sub>TaNb<sub>2</sub>O<sub>10</sub>/(ZnS, PbS) samples were investigated by using FE-SEM techniques. Fig. 1(a) shows the SEM image of HCa<sub>2</sub>Nb<sub>3</sub>O<sub>10</sub> powder containing a number of micron-sized lamellar plates addressed by its crystallographic direction. A very smooth surface was observed for each particle. The solid-state preparation of HCa<sub>2</sub>Nb<sub>3</sub>O<sub>10</sub> formed as aggregates of irregular lamellar plates approximately 300 nm in thickness. From the SEM measurements,

the products after proton exchange by dilute acid for 96 h, the original layered structure was not destroyed.

When the one Nb ion was replaced with one Ta ion, the clearly distinguishable lamellar plates with thicknesses of ca. 20–300 nm were observed in Fig. 1(b). SEM measurements revealed that the shape of the crystallites has been retained in the HCa<sub>2</sub>TaNb<sub>2</sub>O<sub>10</sub> product. The surface texture of the HCa<sub>2</sub>TaNb<sub>2</sub>O<sub>10</sub> was also shown to be rougher than that of HCa<sub>2</sub>Nb<sub>3</sub>O<sub>10</sub>, and the interface between layers were clearly observed for HCa<sub>2</sub>TaNb<sub>2</sub>O<sub>10</sub>. Furthermore, the agglomeration degree less in the HCa<sub>2</sub>TaNb<sub>2</sub>O<sub>10</sub> was observed, which suggested a size reduction. The SEM measurement also revealed that the substituting of Ta ion could suppress the growth of the niobium calcium acid particles.

The plate-like morphology observed for niobates was retained after the intercalation with ZnS and PbS guest, as shown in Fig. 1(c) and (d). The plate-like morphology of niobates was somewhat unsharpened after the intercalation with ZnS and PbS guest; edges and steps of the particles seemed less distinct compared with the sample before intercalation. Comparing with host HCa<sub>2</sub>Nb<sub>3</sub>O<sub>10</sub> and HCa<sub>2</sub>TaNb<sub>2</sub>O<sub>10</sub>, the intercalation compound HCa<sub>2</sub>Nb<sub>3</sub>O<sub>10</sub>/(ZnS, PbS) and HCa<sub>2</sub>TaNb<sub>2</sub>O<sub>10</sub>/(ZnS, PbS) had more debris, and few distinguishable particles small particles. From the SEM micrograph of its cross section, the relatively clear layered structure was observed, indicating that the material was stacked up layer by layer. All the pillared derivatives exhibited an expanded layer stacking in the interlayer direction. This was attributing to the results of the guest species intercalation. The intercalation of *n*-C<sub>6</sub>H<sub>13</sub>NH<sub>2</sub> long chain molecules and pillaring of ZnS and PbS guest in the interlayer spaces led to the expansion of basal spacing, thus inducing lattice deformation. This resulted in the microscopic disintegration of plate-like oxide layers. In addition, layered perovskites have highly anisotropic crystallites and the top-chemical transformations retain this morphology, so it may be possible to design high performance heterojunction photocatalysts.

The composition of the samples determined by Energy-dispersive X-ray spectroscopy (EDS) the distributions of various elements in the selected area corresponding to the SEM image was

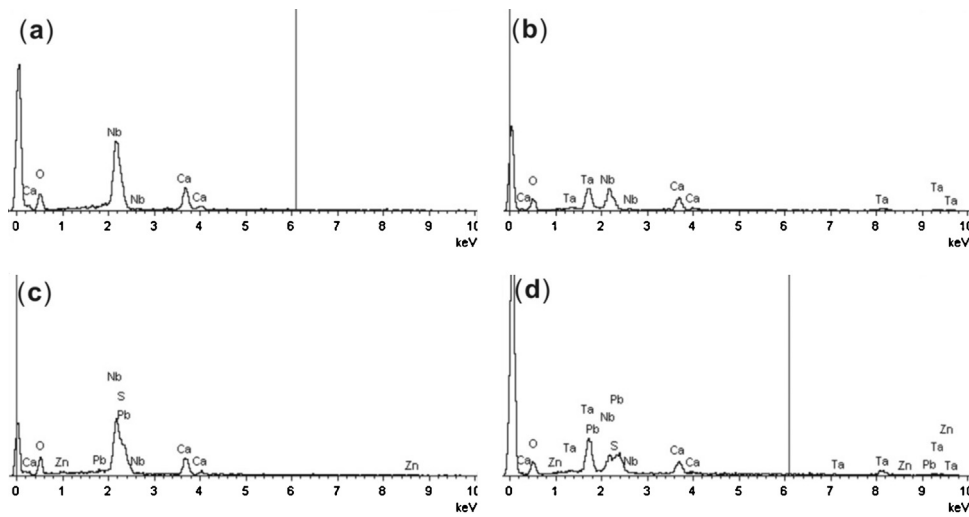


Fig. 2. EDS spectra of (a)  $\text{HCA}_2\text{Nb}_3\text{O}_{10}$ , (b)  $\text{HCA}_2\text{TaNb}_2\text{O}_{10}$ , (c)  $\text{HCA}_2\text{Nb}_3\text{O}_{10}/(\text{ZnS, PbS})$ , and (d)  $\text{HCA}_2\text{TaNb}_2\text{O}_{10}/(\text{ZnS, PbS})$ .

shown in Fig. 2. In the spectrum, peaks associated with Ca, Nb, Ta, O, Zn, Pb, Zn and S were observed. Ca, Nb, and O peaks result from  $\text{HCA}_2\text{Nb}_3\text{O}_{10}$ . The Ta peaks result from  $\text{HCA}_2\text{TaNb}_2\text{O}_{10}$ . The Pb, Zn and S result from PbS and ZnS, respectively. The distribution of the EDS measurements concluded that there was no residual  $\text{K}^+$  in each sample, indicating that interlayer  $\text{K}^+$  ions were substituted by  $\text{H}^+$  cation after proton exchange reaction with dilute acid solution. The samples were likely to be complete protonic niobate. Obviously, the Nb signal intensity of sample  $\text{HCA}_2\text{TaNb}_2\text{O}_{10}$  decreased (Fig. 2b) compared with that of sample  $\text{HCA}_2\text{Nb}_3\text{O}_{10}$  (Fig. 2a). It was due to the partial Nb ion replaced with Ta ion, resulting in the decreasing of Nb peak intensity. Moreover, EDS results further verified that PbS and CdS nanocrystals were successfully intercalated in the interlayer space protonic niobate (Fig. 2c and d). The spectrum confirmed the corresponding chemical elements for composite catalyst and no other elements were detected.

### 3.2. Crystal structure

The synthesis of  $\text{HCA}_2\text{Nb}_3\text{O}_{10}$  with a single phase compositions was confirmed by the X-ray diffractions and shown in Fig. 3a. It

could be seen clearly from Fig. 3a that the as-synthesized layered  $\text{HCA}_2\text{Nb}_3\text{O}_{10}$  was highly crystalline. All of the diffraction lines were matched well with the reported JCPDS Card: 40-0884. The crystal structure of  $\text{HCA}_2\text{Nb}_3\text{O}_{10}$  has tetragonal symmetry with  $a = 0.3850 \text{ nm}$ ,  $c = 1.4379 \text{ nm}$ . The first intense peak observed at  $2\theta$  for the material corresponds to the inter-layer spacing of the sheets (distance between the sheets). According to the X-ray diffraction data, the interlayer distance  $(001) = 1.42 \text{ nm}$ , and the thick of perovskite sheets  $[\text{Ca}_2\text{Nb}_3\text{O}_{10}]^-$  is  $1.16 \text{ nm}$ . The interlayer was bonded by static force. Due to the weaker combination between the interlayer, it was ready to occur intercalate exchange and expand for  $\text{HCA}_2\text{Nb}_3\text{O}_{10}$ . The protons were arranged in the interlayer of  $[\text{Ca}_2\text{Nb}_3\text{O}_{10}]^-$  unit layers, which allowed a ready incorporation of guest molecules and the expansion of the  $c$ -parameter on intercalation. On the other hand,  $\text{HCA}_2\text{Nb}_3\text{O}_{10}$  is a Bronsted acid, and it can react with a base, such as  $\text{C}_3\text{H}_7\text{NH}_2$  and  $\text{C}_6\text{H}_{13}\text{NH}_2$ , to form a supermolecule compound.

The synthesis of  $\text{HCA}_2\text{TaNb}_2\text{O}_{10}$  was confirmed by the X-ray diffractions and shown in Fig. 3b. The XRD patterns of  $\text{HCA}_2\text{TaNb}_2\text{O}_{10}$  photocatalysts were similar to that of  $\text{HCA}_2\text{Nb}_3\text{O}_{10}$  at  $2\theta = 12.3^\circ, 18.5^\circ, 24.7^\circ, 29.7^\circ, 31.1^\circ, 32.9^\circ$ , indicating that the  $\text{Ta}^{5+}$  ions ( $0.068 \text{ nm}$ ) with close ionic radius to the  $\text{Nb}^{5+}$  ( $0.069 \text{ nm}$ ) were substituted into the  $\text{HCA}_2\text{Nb}_3\text{O}_{10}$  lattice. The weak and broad XRD peaks of  $\text{HCA}_2\text{TaNb}_2\text{O}_{10}$  indicate that Nb<sup>5+</sup> being substituted by Ta<sup>5+</sup> induced a decrease in the crystallinity of the  $\text{HCA}_2\text{TaNb}_2\text{O}_{10}$  photocatalysts.

The  $2\theta = 6.1^\circ$  corresponding to  $(001)$  of  $\text{HCA}_2\text{TaNb}_2\text{O}_{10}$  shifted to lower angles than that of  $\text{HCA}_2\text{Nb}_3\text{O}_{10}$ , may be due to the fact that the  $\text{Ta}^{5+}$  radius is a little smaller than that of  $\text{Nb}^{5+}$ , and the distortion of the crystal lattice was induced by substituting Ta for Nb. Under our experimental conditions, the weak peak at  $2\theta = 22.1^\circ$  due to  $\text{Nb}_4\text{Ta}_2\text{O}_{15}$  was observed. It suggested that the appearance of new phase  $\text{Nb}_4\text{Ta}_2\text{O}_{15}$  may be attributed to the replacement of Nb<sup>5+</sup> by excess amounts Ta<sup>5+</sup>.

Because of the cation-exchanging ability of  $\text{HCA}_2\text{Nb}_3\text{O}_{10}$  and derivative, the cation exchange in the impregnation process should result in an intercalation of PbS and ZnS at the cation-exchange site in the interlayer [25,26]. The main peak corresponding to  $(001)$  of  $\text{HCA}_2\text{Nb}_3\text{O}_{10}$  and  $\text{HCA}_2\text{TaNb}_2\text{O}_{10}$  significantly shifted to lower  $2\theta$  angle depending on the species incorporated was shown in Fig. 3c and d, respectively, which was typical for the compound with large interlayer distance. But other diffraction peaks positions of samples (c) and (d) were almost the same as precursors, respectively, which implied that the layered structures were still

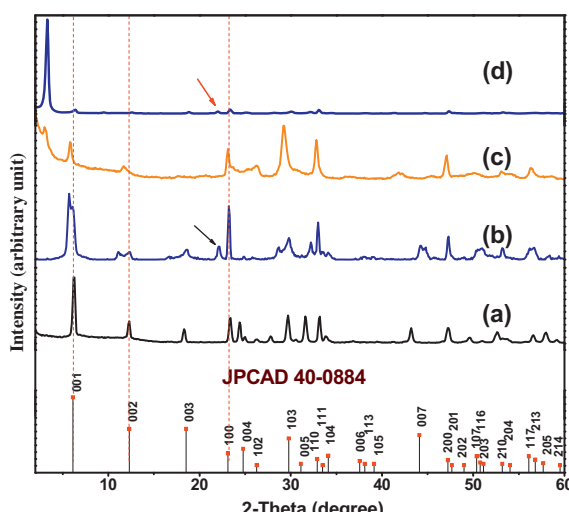
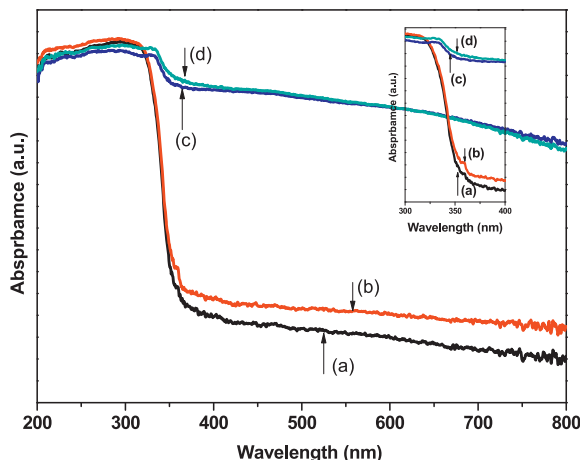


Fig. 3. XRD patterns of (a)  $\text{HCA}_2\text{Nb}_3\text{O}_{10}$ , (b)  $\text{HCA}_2\text{TaNb}_2\text{O}_{10}$ , (c)  $\text{HCA}_2\text{Nb}_3\text{O}_{10}/(\text{ZnS, PbS})$ , (d)  $\text{HCA}_2\text{TaNb}_2\text{O}_{10}/(\text{ZnS, PbS})$ .



**Fig. 4.** UV-vis diffuse reflectance spectra of (a)  $\text{HCA}_2\text{Nb}_3\text{O}_{10}$ , (b)  $\text{HCA}_2\text{TaNb}_2\text{O}_{10}$ , (c)  $\text{HCA}_2\text{Nb}_3\text{O}_{10}/(\text{ZnS, PbS})$  and (d)  $\text{HCA}_2\text{TaNb}_2\text{O}_{10}/(\text{ZnS, PbS})$ .

kept after intercalation of ZnS and PbS. The gallery height of PbS and ZnS determined by subtracting  $\text{HCA}_2\text{Nb}_3\text{O}_{10}$  layer thickness of 1.16 nm from the interlayer distance of  $\text{HCA}_2\text{Nb}_3\text{O}_{10}/(\text{ZnS, PbS})$  of 2.94 nm was 1.78 nm. The gallery height of PbS and ZnS in the interlayer space of  $\text{HCA}_2\text{TaNb}_2\text{O}_{10}/(\text{ZnS, PbS})$  was 1.51 nm. Therefore, the thickness of ZnS and PbS incorporated in the interlayer of  $\text{HCA}_2\text{Nb}_3\text{O}_{10}$  was suggested to be less than 2 nm which indicated that semiconductors confined in the interlayer region of a lamellar compound and an intercalated nanomaterial was formed. The crystallinity also decreased to a great extent as the diffraction peak becomes broad and the intensity declined sharply. The sample  $\text{HCA}_2\text{Nb}_3\text{O}_{10}/(\text{ZnS, PbS})$  and  $\text{HCA}_2\text{TaNb}_2\text{O}_{10}/(\text{ZnS, PbS})$  showed no diffraction peaks corresponding to PbS and ZnS, respectively, indicating that PbS and ZnS were incorporated in the interlayer. This is consistent with the very small particle size and with the non-crystalline nature of the PbS or/and ZnS nanoparticles.

### 3.3. UV-vis spectroscopy of as-prepared samples

**Fig. 4** shows the UV-vis diffuse reflectance spectra of as-prepared samples. The optical band gap of the powders could be estimated from the diffuse reflectance spectra using the following equation [27]:

$$ahv = A(hv - E_g)^{n/2} \quad (2)$$

where  $a$ ,  $v$ ,  $E_g$ , and  $A$  are absorption coefficient, light frequency, band gap, and a constant, respectively. The value of  $n$  decides the characteristics of the transition in a semiconductor ( $n=1$  and 2 for direct interband transition and indirect interband transition, respectively). As shown in **Fig. 5**, the relationship between  $(\alpha h\nu)^2$  and  $(h\nu)$  was plotted. The good linear relationship between  $(\alpha h\nu)^2$  and  $(h\nu)$  implied the direct transition nature for samples. So, the value of  $n$  in Eq. (2) for materials was 1, indicating that a direct optical transition can occur with no significant change in the wave vector for samples. The value of the band gap ( $E_g$ ) was obtained by extrapolating the linear portion of the graphics to the  $h\nu$  axis of the abscissa. We can estimate the band-gap energies of the samples  $\text{HCA}_2\text{Nb}_3\text{O}_{10}$ ,  $\text{HCA}_2\text{TaNb}_2\text{O}_{10}$ ,  $\text{HCA}_2\text{Nb}_3\text{O}_{10}/(\text{ZnS, PbS})$  and  $\text{HCA}_2\text{TaNb}_2\text{O}_{10}/(\text{ZnS, PbS})$  to be 3.66, 3.65, 3.54 and 3.53 eV, respectively.

The sample  $\text{HCA}_2\text{Nb}_3\text{O}_{10}$  possessed a strong absorption in the UV and near-UV region and a weak absorption in the visible region as shown in **Fig. 4(a)**. The sharp absorption edge in the ultraviolet region at about 339 nm was a characteristic band for the

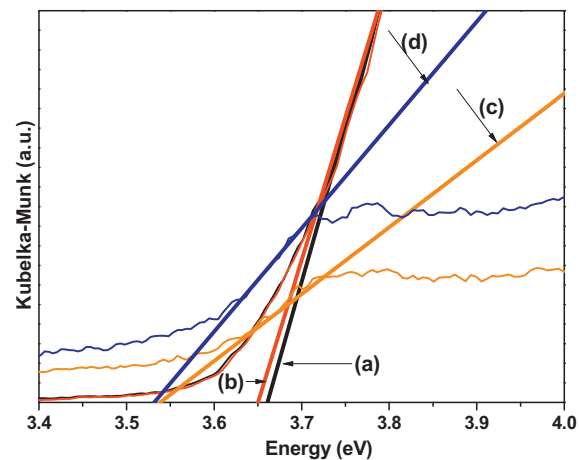


**Fig. 5.** Estimated band gap of (a)  $\text{HCA}_2\text{Nb}_3\text{O}_{10}$ , (b)  $\text{HCA}_2\text{TaNb}_2\text{O}_{10}$ , (c)  $\text{HCA}_2\text{Nb}_3\text{O}_{10}/(\text{ZnS, PbS})$  and (d)  $\text{HCA}_2\text{TaNb}_2\text{O}_{10}/(\text{ZnS, PbS})$  by Kubelka-Munk function. The intercept 3.66, 3.65, 3.54 and 3.53 eV at  $F(R)^2 = 0$  are determined as the band gap of samples (a), (b), (c) and (d), respectively.

calcium niobate nanosheets [ $\text{Ca}_2\text{Nb}_3\text{O}_{10}$ ] due to the electron transitions from the valence band to conduction band ( $\text{O } 2p \rightarrow \text{Nb } 4d$ ) [28].

Compared with the Uv-vis absorption spectra of  $\text{HCA}_2\text{Nb}_3\text{O}_{10}$ , the Uv-vis absorption spectrum of  $\text{HCA}_2\text{TaNb}_2\text{O}_{10}$  shows a similar absorption in the ultraviolet region, as shown in **Fig. 4(b)**, because of the close ionic radius of  $\text{Ta}^{5+}$  and  $\text{Nb}^{5+}$ . However, the slight red shift was clearly observed. The band-gap energy of layered perovskite materials consisting of  $\text{NbO}_6$  octahedral units is affected by several factors including the distortion of  $\text{NbO}_6$  units, the thickness of perovskite layers, and the electronegativity of elements on the octahedral and 12-coordinate sites.  $\text{Ta}^{5+}$  ions in  $\text{HCA}_2\text{TaNb}_2\text{O}_{10}$  replaced  $\text{Nb}^{5+}$  ions to form solid solution. This replacement slightly distorted the crystalline lattice which gave effect on the optical absorption property of the photocatalysts material. For the  $\text{HCA}_2\text{Nb}_3\text{O}_{10}$  and  $\text{HCA}_2\text{TaNb}_2\text{O}_{10}$  samples, the valence band potentials should be the same due to the similar crystal structure. The slight difference of band gaps in the photocatalysts might result from that of the conduction band.  $\text{Ta}^{5+}$  substitution should increase the conduction band level of  $\text{HCA}_2\text{TaNb}_2\text{O}_{10}$ , and lead to the delocalization of the excitation energy due to the distortion of the crystal structure arising from Ta substitution.

Comparing with the sample  $\text{HCA}_2\text{Nb}_3\text{O}_{10}$ , the UV-vis absorption edges of the  $\text{HCA}_2\text{Nb}_3\text{O}_{10}/(\text{ZnS, PbS})$  showed obviously red shift corresponding to a band gap of about 3.54 eV, as shown in **Fig. 4(c)**, which might be due to some changes in the band structure of the materials before and after the intercalation reaction. The Uv-vis absorption spectra of lamellar compound varied according to the intercalated species present in the interlayer of the layered compound. The light absorbance intensity of the  $\text{HCA}_2\text{Nb}_3\text{O}_{10}/(\text{ZnS, PbS})$  in the visible region was greater than that of the precursor  $\text{HCA}_2\text{Nb}_3\text{O}_{10}$ , reflecting that the guest particles produced a very significant influence on the light absorption performance lamellar compound. However, no reflections attributed to ZnS and PbS were observed by the XRD diffraction. The reasonable explanation was that the ZnS and PbS particles intercalated in interlayer of niobate arrayed into 2D structure along the orientation paralleled to the layer and confined at the atom level in the orientation perpendicular to the layer, or the ZnS and PbS embedded in host materials with other ways were in disorder due to the limited interlayer space. This form of ZnS and PbS arrayed in niobate possibly exhibited different optical property from that of the literatures [18,19]. The same phenomenon was also presented on the  $\text{HCA}_2\text{TaNb}_2\text{O}_{10}/(\text{ZnS, PbS})$  samples, as shown in **Fig. 4(d)**. The absorption edge of

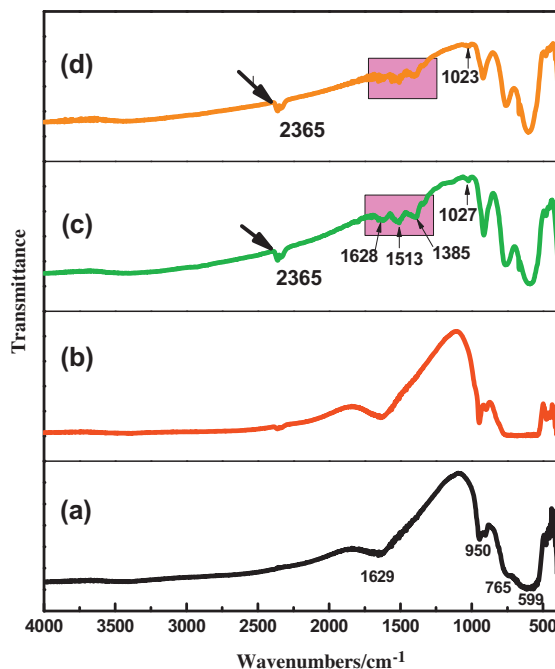


Fig. 6. Fourier transformed infrared (FT-IR) spectra of (a)  $\text{HCA}_2\text{Nb}_3\text{O}_{10}$ , (b)  $\text{HCA}_2\text{TaNb}_2\text{O}_{10}$ , (c)  $\text{HCA}_2\text{Nb}_3\text{O}_{10}/(\text{ZnS, PbS})$  and (d)  $\text{HCA}_2\text{TaNb}_2\text{O}_{10}/(\text{ZnS, PbS})$ .

$\text{HCA}_2\text{Nb}_3\text{O}_{10}/(\text{ZnS, PbS})$  and  $\text{HCA}_2\text{TaNb}_2\text{O}_{10}/(\text{ZnS, PbS})$  appeared a red-shift into the visible light region, which was longer than that of corresponding origin sample. This factor can be attributed to the small particle size (less than interlayer spacing) and small band gap (0.41 eV) of PbS in the composite, and its large exciton Bohr radius of 20 nm, which leads to extensive quantum size effects. It has been reported that the absorption range can be tuned by adjusting the particle size of PbS [29].

It is well known that light absorption by the material and the migration of the light-induced electrons and holes are the most key factors controlling a photocatalytic reaction, which is relevant to the electronic structure characteristics of the material [30,31]. The process for photocatalysis of semiconductor is the direct absorption of photon by band of the materials and generates electron–hole pairs in the semiconductor particles. The excitation of an electron from the valence band to the conduction band is initiated by light absorption with energy equal to or greater than the band gap of the semiconductor. Upon excitation, the photogenerated electron and hole can migrate to the surface of semiconductor. It is namely that the narrower band gap of the semiconductor can harvest more photons to excite the electron from the valence band to the conduction band.

#### 3.4. FT-IR spectra of as-prepared samples

Fourier transformed infrared spectroscopy (FT-IR) is a widely used technique in the study of the substructure of layered compound and can be used to monitor the conformational changes when the guests were incorporated into the interspaces of layered compound. The characteristic vibration bands due to  $[\text{Ca}_2\text{Nb}_3\text{O}_{10}]^{-1}$  layer were seen between 450 and 1000 cm<sup>-1</sup> in the all layered compounds. Absorption peaks appearing at 599, 765 and 950 cm<sup>-1</sup> for the  $[\text{Ca}_2\text{Nb}_3\text{O}_{10}]^{-1}$  layer were assigned to the asymmetric stretching vibration of  $\text{Nb}-\text{O}_{\text{bridge}}$  in central  $\text{NbO}_6$  octahedron, asymmetric stretching vibration of  $\text{Nb}-\text{O}_{\text{bridge}}$  in terminal  $\text{NbO}_6$  octahedron, stretching vibration of  $\text{Nb}-\text{O}_{\text{terminal}}$  vibrations [32,33], respectively, as shown in Fig. 6a. And the band

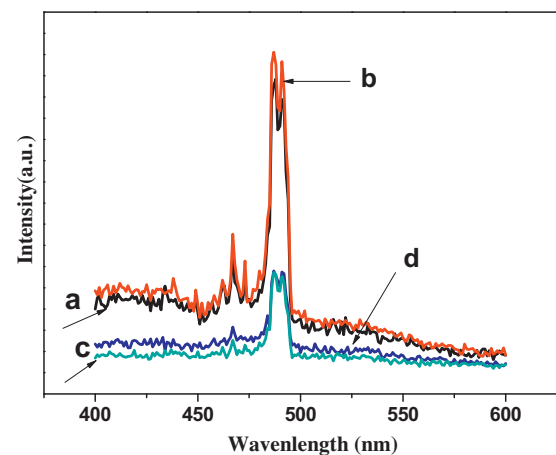


Fig. 7. Photoluminescence (PL) spectra of the samples (under 455 nm photoexcitation) at room temperature, (a)  $\text{HCA}_2\text{Nb}_3\text{O}_{10}$ , (b)  $\text{HCA}_2\text{TaNb}_2\text{O}_{10}$ , (c)  $\text{HCA}_2\text{Nb}_3\text{O}_{10}/(\text{ZnS, PbS})$  and (d)  $\text{HCA}_2\text{TaNb}_2\text{O}_{10}/(\text{ZnS, PbS})$ .

at 1629 cm<sup>-1</sup> was recognized as the stretching and bending vibrations of hydroxyl group. Substitution has a slight effect on the FT-IR spectra of  $\text{HCA}_2\text{TaNb}_2\text{O}_{10}$  compound. The shifts in peak positions and changes in the intensity were observed as a consequence of substitution. The FT-IR bands were broader for substituted compound  $\text{HCA}_2\text{TaNb}_2\text{O}_{10}$  than for  $\text{HCA}_2\text{Nb}_3\text{O}_{10}$  precursor perhaps due to the changes in molecular geometry and lowered symmetry of the host layer in the former compound.

The three bands of Nb–O of the samples (c) and (d) were sharper and stronger than those of samples (a) and (b), respectively, indicating a smaller distortion of the structure after the guest particles intercalation. The faint peak at 1023 or 1027 cm<sup>-1</sup> was likely the S–O stretch [29]. The weak bands and shoulders at 2365, 1628, 1513, 1385 and 1027 cm<sup>-1</sup> might be due to the nano-structural formation of the sulfides in the interlayer space of layered compound, which was analogous to that of the previous report [34]. The characteristic vibration peaks of the Zn–S bond at 655 and Pb–S 6771 cm<sup>-1</sup> were not detected in our experiments [35,36]. This was because the former (655 cm<sup>-1</sup>) was too weak to be resolved, and the latter (6771 cm<sup>-1</sup>) was beyond our detection limit.

#### 3.5. Fluorescence of samples

In general, the photoluminescence (PL) technique has been widely used to investigate the electronic structure, optical and photochemical properties of semiconductor materials, by which information such as surface oxygen vacancies and defects, as well as the efficiency of charge carrier trapping, immigration and transfer can be obtained. In this paper, we investigated the efficiency of charge carrier trapping, immigration and transfer at the surface of semiconductors to understanding the annihilation of electron–hole pairs in semiconductors particles. Fig. 7 shows the PL spectra of the as-prepared samples measured at room temperature at an excitation wavelength of 455 nm. When excite the sample at 455 nm, the broad emission peaks centered at 488 nm were observed for all the samples of  $\text{HCA}_2\text{Nb}_3\text{O}_{10}$ ,  $\text{HCA}_2\text{TaNb}_2\text{O}_{10}$ ,  $\text{HCA}_2\text{Nb}_3\text{O}_{10}/(\text{ZnS, PbS})$  and  $\text{HCA}_2\text{TaNb}_2\text{O}_{10}/(\text{ZnS, PbS})$  powders, suggesting that the emission centre is the perovskite layer consisting of  $\text{NbO}_6$  units [37,38]. Because the luminescence wavelength ranges are similar, the visible emission should be intrinsic in origin for  $\text{HCA}_2\text{Nb}_3\text{O}_{10}$  and corresponding to a self-trapped exciton, such as  $\text{Nb}^{4+}-\text{O}^-$  state in  $\text{NbO}_6$  octahedral. In comparison with the absorption spectra, the Stokes shift of PL is large for these  $\text{HCA}_2\text{Nb}_3\text{O}_{10}$  specimens. The large Stokes shifts can be ascribed to a strong electron–lattice interaction and exciton relaxation. Besides the fact that the nature of the ion

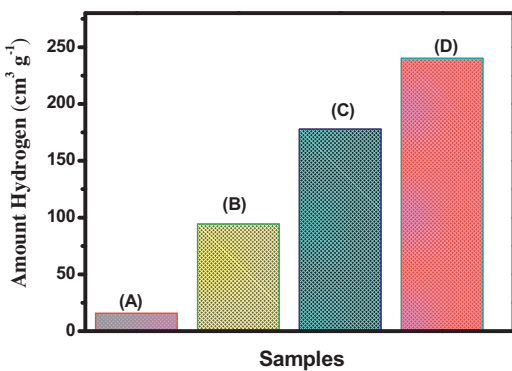


**Fig. 8.** Amount of  $\text{H}_2$  produced from  $500 \text{ cm}^3$  of  $\text{Na}_2\text{S}$  ( $0.2 \text{ mol dm}^{-3}$ ) and  $\text{Na}_2\text{SO}_3$  ( $0.2 \text{ mol dm}^{-3}$ ) aqueous solution containing  $1.0 \text{ g}$  of dispersed (A)  $\text{HCA}_2\text{Nb}_3\text{O}_{10}$ , (B)  $\text{HCA}_2\text{TaNb}_2\text{O}_{10}$ , (C)  $\text{HCA}_2\text{Nb}_3\text{O}_{10}/(\text{ZnS, PbS})$  and (D)  $\text{HCA}_2\text{TaNb}_2\text{O}_{10}/(\text{ZnS, PbS})$  by irradiating with a  $300 \text{ W}$  Hg illumination system for  $1 \text{ h}$ .

in the 12-coordination site in the perovskite-like layers can change the photochemical behavior of niobates, it has been observed that other materials properties are dependent of the metal ion in the niobate layers. Thus it was reasonable that the fluorescence intensity of sample  $\text{HCA}_2\text{TaNb}_2\text{O}_{10}$  was strong than that of  $\text{HCA}_2\text{Nb}_3\text{O}_{10}$  [39].

It should be noted that the emission intensity of sample  $\text{HCA}_2\text{Nb}_3\text{O}_{10}/(\text{ZnS, PbS})$  and  $\text{HCA}_2\text{TaNb}_2\text{O}_{10}/(\text{ZnS, PbS})$  were much stronger than that of corresponding native host, respectively. It is known that the luminescence properties of niobates are strongly dependent of theirs structure. For such systems,  $\text{HCA}_2\text{Nb}_3\text{O}_{10}$  and  $\text{HCA}_2\text{TaNb}_2\text{O}_{10}$  built up from corner-sharing octahedral as the perovskite-like ones, show weak luminescence. The increase of emission intensity can be attributed to the decrease of rate constants of electron hole recombination by non-radiative processes, i.e. the decrease of the defects that act as non-radiative electron and hole recombination centers [38,40].

### 3.6. Photocatalytic properties of as-prepared samples

The amount of hydrogen evolution from  $500 \text{ cm}^3$  of  $\text{Na}_2\text{S}$  ( $0.2 \text{ mol dm}^{-3}$ ) and  $\text{Na}_2\text{SO}_3$  ( $0.2 \text{ mol dm}^{-3}$ ) aqueous solution containing  $1.0 \text{ g}$  of as-prepared samples powder dispersed in at  $60^\circ\text{C}$  for  $1 \text{ h}$  under irradiation from a  $300 \text{ W}$  mercury lamp is shown in Fig. 8. The gas produced was ascertained as hydrogen gas by analysis with gas chromatography. The reaction stopped when the light was turned off in this experiment, showing the obvious light response, it was confirmed that no reaction occur in the dark. The result of photocatalytic reaction showed that the photocatalytic reaction was induced by the absorption of light irradiation. The total amount of  $\text{H}_2/\text{catalyst}$  (mol) for these photocatalysts was much greater than  $1.0$ , indicating that the reaction occurs catalytically. After an abdication period less than  $0.5 \text{ h}$ , gas evolved steadily. No photocorrosion was observed in the present system evidenced from the atomic absorption analysis for  $\text{Pb}^{2+}$  and  $\text{Zn}^{2+}$  ions in the filtrate after water splitting reaction. The photocatalytic activity of photocatalyst still keeps  $90\%$  which was stocked in the dark  $30 \text{ days}$ . The amount of hydrogen gas evolved increase in the sequence:  $\text{HCA}_2\text{Nb}_3\text{O}_{10} < \text{HCA}_2\text{TaNb}_2\text{O}_{10} < \text{HCA}_2\text{Nb}_3\text{O}_{10}/(\text{ZnS, PbS}) < \text{HCA}_2\text{TaNb}_2\text{O}_{10}/(\text{ZnS, PbS})$ . The lowest activity was observed over  $\text{HCA}_2\text{Nb}_3\text{O}_{10}$  under the present experiment conditions.

It has been shown that the band gap of  $\text{HCA}_2\text{TaNb}_2\text{O}_{10}$  is close to that of  $\text{HCA}_2\text{Nb}_3\text{O}_{10}$ . However, the photocatalytic activities of  $\text{HCA}_2\text{TaNb}_2\text{O}_{10}$  are still higher than that of the pure  $\text{HCA}_2\text{Nb}_3\text{O}_{10}$ . It is well known that the distorted crystal structures provide local polarization fields; accordingly, separation and transport of the photogenerated charge occur efficiently. Therefore, it is considered

that  $\text{HCA}_2\text{TaNb}_2\text{O}_{10}$  has higher charge separation efficiency than  $\text{HCA}_2\text{Nb}_3\text{O}_{10}$ , due to distorted crystal structure [41]. The finding is in agreement with the result obtained from the UV-vis spectrum of samples. Furthermore, according to the PL spectrum, the excitonic PL intensity of  $\text{HCA}_2\text{TaNb}_2\text{O}_{10}$  was increased by replacing partial Nb ion with Ta ion, which can result in an increase in the content of surface oxygen vacancy and defect. As a result,  $\text{HCA}_2\text{TaNb}_2\text{O}_{10}$  showed higher photocatalytic water splitting performance than  $\text{HCA}_2\text{Nb}_3\text{O}_{10}$ .

The amount of  $\text{H}_2$  evolutions over  $\text{HCA}_2\text{Nb}_3\text{O}_{10}$  were significantly increased by the intercalation of  $\text{PbS}$  and  $\text{ZnS}$  into the interlayer space of the perovskite sheet as shown in Fig. 8. Therefore, the  $\text{PbS}$  and  $\text{ZnS}$  pillar which was incorporated in the interlayer played an important part in photocatalytic water cleavage. The promotion effect was maybe attributed to the formation of the  $\text{PbS}$  and  $\text{ZnS}$  nanoparticles incorporated in the interlayer, as well as the micro-heterojunctions between the host layer and the  $\text{PbS}$  and  $\text{ZnS}$ . The incorporation of  $\text{PbS}$  and  $\text{ZnS}$  nanoparticles into the interlayer of these layered metal oxides could suppress the particle growth. Nanoscale guest particles induced a quantum size effect. Photogenerated electrons could quickly be transferred through the nanostructure, and the recombination between the photoinduced charge carriers (electron and hole) was effectively depressed. Consequently, the photocatalytic evolution of hydrogen was enhanced.

Better photocatalytic stability of intercalated material than unsupported material was due to the semiconductor catalyst was anchored in the interlayer of heteropoly acid compound. The incorporated  $\text{PbS}$  and  $\text{ZnS}$  nano-particles had a good contact between guest and  $[\text{Ca}_2\text{Nb}_3\text{O}_{10}]$  host layers. On the other hand, the coupling of two semiconductor particles with different energy level was useful to achieve effective charge separation. In  $\text{HCA}_2\text{Nb}_3\text{O}_{10}/\text{MS}$ , a photo-generated electron could transfer from the guest MS particles to the  $[\text{Ca}_2\text{Nb}_3\text{O}_{10}]$  host layers, while the holes remained in the guest MS particles. This helped to diffuse the electrons and holes before reaching the interface, and the holes and electrons could be effectively captured by the electrolyte in the solution.

In addition, the narrow band gap semiconductor  $\text{PbS}$  ( $0.4 \text{ eV}$ ) could not only restrain the recombination of electrons and holes, but also expended the spectral response region. It was beneficial to improving the efficiency of photocatalytic reaction. Upon photoexcitation, electrons and holes were generated in the sheets, causing redox reactions with reactant molecules adjacent to the layers. Therefore, the primary requirement to achieve high efficiency using a layered photocatalyst was the intercalation of reactant molecules (e.g.,  $\text{H}_2\text{O}$ ) into the interlayer galleries, because of enhanced access of photogenerated carriers to reactants. Furthermore,  $\text{ZnS}$  in itself is a highly active photocatalyst for  $\text{H}_2$  evolution from aqueous solutions containing sacrificial reagents such as  $\text{SO}_3^{2-}$  and  $\text{S}^{2-}$  without noble metal such as  $\text{Pt}$  [42], indicating that the surface of  $\text{ZnS}$  possesses active sites for  $\text{H}_2$  evolution.

In all samples,  $\text{PbS}$  and  $\text{ZnS}$  co-intercalated  $\text{HCA}_2\text{TaNb}_2\text{O}_{10}$  photocatalyst showed the highest activity. This might also suggest that the synergistic effect of nano-sized  $\text{ZnS}$  and  $\text{PbS}$  in the  $\text{HCA}_2\text{TaNb}_2\text{O}_{10}$  photocatalysts was an important factor for the improvement of photocatalytic efficiency. In addition, the substitution of Ta for partial Nb in the layered composite brought the quick transference of the electrons in a  $\text{ZnS}$  and  $\text{PbS}$  pillar through the  $\text{HCA}_2\text{TaNb}_2\text{O}_{10}$  layer into the surface of photocatalysts. The guest-to-host charge transfer was also consistent with the phenomena presented from PL spectrum. The substitution of Ta for partial Nb in the  $\text{HCA}_2\text{TaNb}_2\text{O}_{10}$  increased significantly the amount of intercalated reactant. An explanation might be that a decrease of the charge densities in the interlayer due to the substitution could facilitate the intercalation reaction in the interlayer [43]. Consequently, the amount of  $\text{H}_2$  is produced highly.

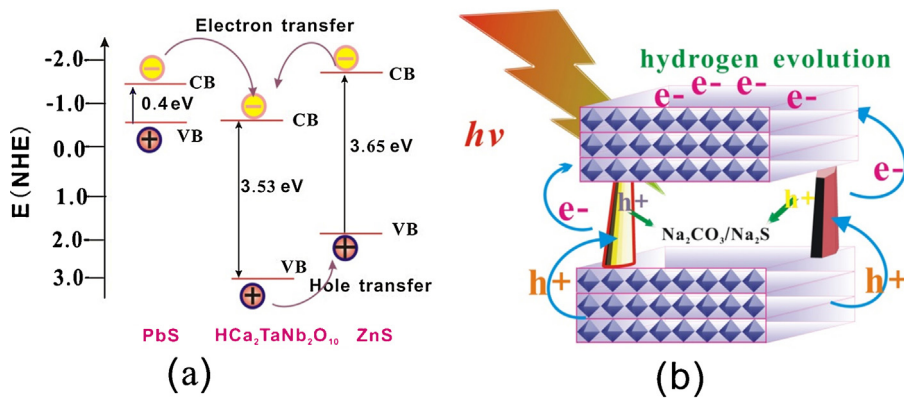
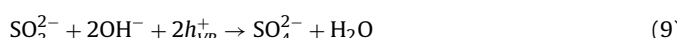
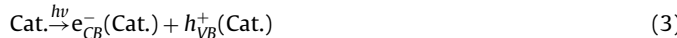


**Fig. 9.** (a) Energy levels of the conduction and valence band edges vs. normal hydrogen electrode (NHE, at pH = 0) for ZnS, HCa<sub>2</sub>TaNb<sub>2</sub>O<sub>10</sub> and PbS. (b) Schematic illustration for the charge transfer and separation in HCa<sub>2</sub>TaNb<sub>2</sub>O<sub>10</sub>/(ZnS, PbS) under light irradiation.

### 3.7. Photocatalytic reaction mechanism

It is accepted that the energy band of photocatalyst semiconductor is composed of a low-energy valence band full of electrons and a high-energy conduction band with no electron. When photocatalyst absorbs the photons with energy greater than its band gap to generate electron/hole pairs, and the electrons are excited to conduction band ( $e_{CB}^-$ ) and left the holes in valence band ( $h_{VB}^+$ ) (Eq. (3)) [44–46]. Then, both the photogenerated electrons and holes may migrate to the surfaces of the catalyst particles and proceed with oxidation–reduction reactions, respectively, with the locally absorbed species.



For preventing photogenerated electrons from recombining with photogenerated holes is to scavenge the holes with sacrificial electron donors. Therefore, an electron donor system, Na<sub>2</sub>S/Na<sub>2</sub>SO<sub>3</sub>, was employed in our work to scavenge the holes generated in the valence band of the composite photocatalyst. In the absence of oxygen and presence of sacrificial species such as S<sup>2-</sup>, the holes in valence band were trapped by S<sup>2-</sup> to yield S (Eq. (5)), while the electrons in conduction band reduced water and/or protons in the solution to form hydrogen as shown by Eq. (4). The aqueous SO<sub>3</sub><sup>2-</sup> added could dissolve S into S<sub>2</sub>O<sub>3</sub><sup>2-</sup> in order to prevent any detrimental deposition of S onto photocatalysts (Eq. (6)). Therefore, the photocorrosion of guest MS particles was prevented. The S<sup>2-</sup> could consume the holes effectively and generate S<sub>2</sub><sup>-</sup>, which was in turn recycled to S<sup>2-</sup> by SO<sub>3</sub><sup>2-</sup>, as shown in Eqs. (7) and (8). At the same time, the production of S<sub>2</sub><sup>-</sup>, which competed with the reduction of protons, was efficiently suppressed by mixing with SO<sub>3</sub><sup>2-</sup>. Furthermore, some SO<sub>3</sub><sup>2-</sup> ions could also be oxidized by the

photogenerated holes to form SO<sub>4</sub><sup>2-</sup> (Eq. (9)). Thus, H<sub>2</sub> evolved with the reduction of water molecules by photogenerated electrons.



It is notable that these reactions simultaneously compete with the recombination of the photoinduced electrons and holes (Eq. (10)), and the recombination reactions debase the efficiency of photocatalytic reaction. In intercalated material, the photoinduced electrons could quickly be transferred through the host, and the recombination (Eq. (10)) between the photoinduced charge carriers was effectively depressed. This was one of the reasons that HCa<sub>2</sub>TaNb<sub>2</sub>O<sub>10</sub>/(ZnS, PbS) intercalated material has higher photocatalytic activity than that of unsupported HCa<sub>2</sub>TaNb<sub>2</sub>O<sub>10</sub>.

The conduction band edge potential of a semiconductor is one of the important parameters affecting the overall efficiency of H<sub>2</sub> production from water. The bottom level of the conduction band has to be more negative than the redox potential of H<sup>+</sup>/H<sub>2</sub> (0 V vs. NHE), while the top level of the valence band be more positive than the redox potential of O<sub>2</sub>/H<sub>2</sub>O (1.23 V). The relationship between the conduction band potential ( $E_{CB}$ ) of metal–oxide semiconductors containing d<sup>0</sup> and d<sup>10</sup> metal ions and the band gaps ( $E_g$ ) can be roughly represented by the following equations:

$$E_{CB} = 1.23 - \frac{E_g}{2} \quad (11)$$

The bandgap of HCa<sub>2</sub>TaNb<sub>2</sub>O<sub>10</sub> was estimated to be about 3.53 eV from the UV–vis diffuse reflectance spectrum. Therefore, the conduction band (CB) levels were around 0.54 V vs. NHE. The band gap of PbS was estimated to be about 0.40 eV. The band gap of ZnS was estimated to be about 3.65 eV. Thus, we could estimate the conduction band potentials of HCa<sub>2</sub>TaNb<sub>2</sub>O<sub>10</sub>, ZnS and PbS from their band-gap energies. According to the relative position of the valence bands and conduction bands for HCa<sub>2</sub>TaNb<sub>2</sub>O<sub>10</sub>, ZnS and PbS, the band structure of HCa<sub>2</sub>TaNb<sub>2</sub>O<sub>10</sub>/(ZnS, PbS) was determined, and are schematically illustrated in Fig. 9a.

The photocatalyst ZnS, PbS and HCa<sub>2</sub>TaNb<sub>2</sub>O<sub>10</sub> generated electrons and holes together under light irradiation as shown in Fig. 9b. The photogenerated electrons on the conduction band of ZnS and PbS could migrate to the conduction band of HCa<sub>2</sub>TaNb<sub>2</sub>O<sub>10</sub> with the higher potential, and the photogenerated holes on the valence band of HCa<sub>2</sub>TaNb<sub>2</sub>O<sub>10</sub> could migrate to the valence band of ZnS with the lower potential. Thus, photogenerated electrons accumulated in the conduction band of HCa<sub>2</sub>TaNb<sub>2</sub>O<sub>10</sub> and holes accumulated in the valence band of ZnS and PbS, which facilitated the separation of the photogenerated electron–hole pairs and acted to improve the photocatalytic activity. Consequently, the photogenerated electron could effectively reduce H<sub>2</sub>O (or H<sup>+</sup>) to produce

$H_2$ . The photogenerated holes could be scavenged by the sacrificial electron donor system ( $Na_2S/Na_2SO_3$ ).

#### 4. Conclusions

In summary, from the results of tests described, the following conclusions may be drawn:  $ZnS$  together with  $PbS$  were incorporated into the interlayer of  $HCa_2Ta_xNb_{3-x}O_{10}$  ( $x=0, 1$ ) by successive reaction of  $HCa_2Ta_xNb_{3-x}O_{10}$ , with  $n-C_6H_{13}NH_2/C_2H_5-OH$  organic solution, and with  $Zn(CH_3COO)_2$  and  $Pb(CH_3COO)_2$  aqueous solution, respectively, followed introducing  $H_2S$  gas. The gallery height of  $PbS$  and  $ZnS$  d pillar in  $HCa_2Ta_xNb_{3-x}O_{10}/(ZnS, PbS)$  nanocomposites was less than 2 nm. The photocatalytic activity of  $HCa_2Ta_xNb_{3-x}O_{10}/(ZnS, PbS)$  intercalated material was superior to those of unsupported  $HCa_2Ta_xNb_{3-x}O_{10}$ . As a result,  $HCa_2TaNb_2O_{10}/(ZnS, PbS)$  showed highest photocatalytic water splitting performance than other samples, and this is mainly due to its better guest-to-host charge transfer separation efficiency and higher conduction band edge position caused by the substitution of  $Ta$  for partial  $Nb$  in the  $HCa_2TaNb_2O_{10}$ .

#### Acknowledgment

The project was jointly supported by the National Natural Science Foundation of China (No. 61306077), the Provincial National Science Foundation of Fujian Province (2013J01188), National Science Foundation of Quanzhou City (2011G4) and the Fundamental Research Funds for the Central Universities (JB-ZR1109, JB-ZR1212).

#### References

- [1] X.B. Chen, S.H. Shen, L.J. Guo, S.S. Mao, *Chem. Rev.* 110 (2010) 6503–6570.
- [2] A. Kudo, Y. Miseki, *Chem. Soc. Rev.* 38 (2009) 253–278.
- [3] A. Fujishima, K. Honda, *Nature* 238 (1972) 37–38.
- [4] Y.L. Lai, M. Meng, Y.F. Yu, X.T. Wang, T. Ding, *Appl. Catal., B* 105 (2011) 335–345.
- [5] H. Tong, S.X. Ouyang, Y.P. Bi, N. Umezawa, M. Oshikiri, J.H. Ye, *Adv. Mater.* 24 (2012) 229–251.
- [6] I. Tsuji, H. Kato, H. Kobayashi, A. Kudo, *J. Am. Chem. Soc.* 126 (2004) 13406–13413.
- [7] G. Ma, H. Yan, J. Shi, X. Zong, Z. Lei, C. Li, *J. Catal.* 260 (2008) 134–140.
- [8] R. Chitrakar, S. Tezuka, A. Sonoda, H. Kakita, K. Sakane, K. Ooi, T. Hirotsu, *Ind. Eng. Chem. Res.* 47 (2008) 176–179.
- [9] S.J. Liang, L.J. Shen, J. Zhu, Y.F. Zhang, X.X. Wang, Z.H. Li, L. Wu, X.Z. Fu, *RSC Adv.* 1 (2011) 458–467.
- [10] K.I. Shimizu, Y. Tsuji, T. Hatamachi, K. Toda, T. Kodama, M. Sato, Y. Kitayama, *Phys. Chem. Chem. Phys.* 6 (2004) 1064–1069.
- [11] X. Zong, C. Sun, Z. Chen, A. Mukherji, H. Wu, J. Zou, S.C. Smith, G.Q. Lu, L. Wang, *Chem. Commun.* 47 (2011) 6293–6295.
- [12] O.C. Compton, C.H. Mullet, S. Chiang, F.E. Osterloh, *J. Phys. Chem. C* 112 (2008) 6202–6208.
- [13] N.Z. Bao, L.M. Shen, T. Takata, K. Domen, *Chem. Mater.* 20 (2008) 110–117.
- [14] H. Yan, J. Yang, G. Ma, G. Wu, X. Zong, Z. Lei, J. Shi, C. Li, *J. Catal.* 266 (2009) 165–168.
- [15] A. Kudo, *Int. J. Hydrogen Energy* 32 (2007) 2673–2678.
- [16] N.K. Mudugamuwa, D.M.N.M. Dissanayake, A.A.D.T. Adikaari, S.R.P. Silva, *Sol. Energy Mater. Sol. Cells* 93 (2009) 549–551.
- [17] C. Ratanawananate, Y. Tao, K.J. Balkus Jr., *J. Phys. Chem. C* 113 (2009) 10755–10760.
- [18] R.J. Ellingson, M.C. Beard, J.C. Johnson, P. Yu, O.I. Micic, A.J. Nozik, A. Shabaei, A.L. Efros, *Nano Lett.* 5 (2005) 865–871.
- [19] Y. Zhang, N. Zhang, Z.R. Tang, Y.J. Xu, *ACS Nano* 6 (2012) 9777–9789.
- [20] W. Zhang, X. Zhong, *Inorg. Chem.* 50 (2011) 4065–4072.
- [21] N. Biswal, D.P. Das, S. Martha, K.M. Parida, *Int. J. Hydrogen Energy* 36 (2011) 13452–13460.
- [22] M. Antoniadou, V.M. Dascalaki, N. Balis, D.I. Kondaridesb, C. s Kordulis, P. Lianos, *Appl. Catal., B* 107 (2011) 188–196.
- [23] J. Yu, L. Qi, M. Jaroniec, *J. Phys. Chem. C* 114 (2010) 13118–13125.
- [24] E.M. Sabio, R.L. Chamousis, N.D. Browning, F.E. Osterloh, *J. Phys. Chem. C* 116 (2012) 3161–3170.
- [25] Y.F. Chen, S.H. Zhou, X.J. Yang, Y. OuYang, *J. Solid State Chem.* 183 (2010) 823–828.
- [26] W.Q. Cui, L.Y. Li, Y.F. Liu, J.S. Hu, Y.H. Liang, *Chin. J. Inorg. Chem.* 28 (2012) 773–778.
- [27] G. Cao, L.K. Rabenberg, C.M. Nunn, T.E. Mallouk, *Chem. Mater.* 3 (1991) 149–156.
- [28] H. Zhou, E.M. Sabio, T.K. Townsend, T. Fan, D. Zhang, F.E. Osterloh, *Chem. Mater.* 22 (2010) 3362–3368.
- [29] C. Ratanawananate, C. Xiong, K.J. Balkus Jr., *ACS Nano* 2 (2008) 1682–1688.
- [30] R. Asahi, T. Morikawa, T. Ohwaki, K. Aoki, Y. Taga, *Science* 293 (2001) 269–271.
- [31] H.M. Chen, C.K. Chen, R.S. Liu, L. Zhang, J. Zhang, D.P. Wilkinson, *Chem. Soc. Rev.* 41 (2012) 5654–5671.
- [32] Y. Narendar, G.L. Messing, *Chem. Mater.* 9 (1997) 580–587.
- [33] K. Saruwatari, H. Sato, T. Idei, J. Kameda, A. Yamagishi, A. Takagaki, K. Domen, *J. Phys. Chem. B* 109 (2005) 12410–12416.
- [34] B.S.R. Devi, R. Raveendran, A.V. Vaidyan, *Indian Acad. Sci.* 68 (2007) 679–687.
- [35] R. John, S.S. Florence, *Chalcogenide Lett.* 7 (2010) 269–273.
- [36] P. Zhao, J. Wang, G. Cheng, K. Huang, *J. Phys. Chem. B* 110 (2006) 22400–22406.
- [37] A. Kudo, E. Kaneko, *J. Mater. Sci. Lett.* 16 (1997) 224–226.
- [38] S. Tawkaew, Y. Fujishiro, S. Yin, T. Sato, *Colloids Surf., A* 179 (2001) 139–144.
- [39] S. Muthukumaran, R. Gopalakrishnan, *Opt. Mater.* 34 (2012) 1946–1953.
- [40] Y. Fukugami, T. Sato, *J. Alloys Compd.* 312 (2000) 111–116.
- [41] Y. Inoue, *Energy Environ. Sci.* 2 (2009) 364–386.
- [42] A. Kudo, M. Sekizawa, *Chem. Commun.* 15 (2000) 1371–1372.
- [43] A.B. Marcos, A.L. Shiguihara, V.R.L. Constantino, *J. Mater. Chem.* 19 (2009) 2512–2525.
- [44] J. Bai, J.H. Li, Y.B. Liu, B.X. Zhou, W.M. Cai, *Int. J. Hydrogen Energy* 14 (2010) 408–413.
- [45] K.M. Parida, N. Biswal, D.P. Das, S. Martha, *Int. J. Hydrogen Energy* 36 (2010) 5262–5269.
- [46] J.F. Reber, K. Meier, *J. Phys. Chem.* 88 (1984) 5903–5913.